JOURNAL OF MATERIALS SCIENCE 31 (1996) 3459–3467

The role of grain boundary sliding and reinforcement morphology on the creep deformation behaviour of discontinuously reinforced composites

S. B. BINER
Ames Laboratory, Iowa State University, Ames, IA 50011 USA

In this study, the role of grain boundary sliding behaviour on the creep deformation characteristics of discontinuously reinforced composites is investigated numerically together with the other influencing parameters: reinforcement aspect ratio, grain size and interfacial behaviour between the reinforcement and the matrix. The results obtained for the composites are compared with results obtained for a polycrystalline matrix material having identical grain size and morphology. The results indicate that, with sliding grain boundaries, the stress enhancement factor for the composites is much higher than the one observed for the matrix material and its value increases with increasing reinforcement aspect ratio, reduction in the matrix grain size and sliding interfacial behaviour between the reinforcement and the matrix. In the composites, the contribution of the grain boundary sliding to overall steady state creep rates occurs in a larger stress range in comparison to the matrix material. Experimentally observed higher creep exponent values or stress dependent creep exponent values for the composites could not be explained solely by the mechanism of grain boundary sliding. However, experimentally observed large scale triple point grain boundary cavitation in the composites could occur due to large grain rotations resulting from grain boundary sliding.

1. Introduction

Discontinuously reinforced composites are under development to meet the requirements of advanced structural applications which will operate at elevated temperatures. To achieve these objectives different avenues are being explored, including efforts for increasing fracture toughness of normally brittle ceramics by addition of reinforcements [1], development of intermetallic composites [2, 3] and metal matrix composites [4]. In these newly engineered materials much of the effort has been spent understanding the micromechanism of room temperature deformation and fracture [5, 6]; very little work has been done to understand their micromechanism of time-dependent deformation and failure at elevated temperatures [7, 8]. However, a good understanding of micromechanisms for both temperature ranges could be most valuable in the design of these composite systems through intelligent manipulation of microstructure.

Several effects of grain boundary sliding on the deformation behaviour of polycrystalline solids at creep regime have been widely recognized. The creep strain rate becomes slightly higher in the low stress, low strain rate regime as a result of grain boundary sliding [9–12]. The creep constitutive equation for non-sliding homogenous polycrystalline solids can be characterized by the power law equation,

$$\dot{\varepsilon}_c = \dot{\varepsilon}_o \left(\frac{\sigma_e}{\sigma_o}\right)^n \quad (1)$$

where σ_o is the reference stress, $\dot{\varepsilon}_0$ is a temperature dependent reference strain rate, n is the creep exponent and σ_e is the equivalent stress. For sliding grain boundaries the corresponding equation is:

$$\dot{\varepsilon}_c = \dot{\varepsilon}_o \left(f\frac{\sigma_e}{\sigma_o}\right)^n \quad (2)$$

where f ($f > 1$) is usually called the *stress enhancement factor*. The effect of grain boundary sliding on the overall creep rate of non-cavitating polycrystalline materials has been studied by using spring models [12], for a two dimensional array of hexagonal grains by using a finite element model (FEM) [9–11] and utilizing the self consistent method [13]. A three dimensional Wigner–Seitz cell has been also investigated by applying a minimum energy principle to an approximate stress distribution [14] and applying the FEM technique [15]. From these studies, it appears that f does not depend on the grain size, but may

0022–2461

depend on the geometrical parameters related to the grain shape. Although in an earlier analysis [9], f values were found to be independent of the creep exponent n (having values of 1.1 ∓ 0.01 for $1 \leqslant n \leqslant 8.8$) more recent studies [10, 11] have shown a larger value and a slight increase in f with increasing creep exponent (1.1 to 1.26 for $1 \leqslant n \leqslant 8$). On the other hand, the FEM analysis for determination of stress enhancement factor using three dimensional Wigner–Seitz unit-cells for a polycrystalline material have shown larger values of the stress enhancement factor but decreasing behaviour with increasing creep exponent (1.31 to 1.23 for $1 \leqslant n \leqslant 7$) [15]. Although the stress enhancement factor has been evaluated by several authors [9–15] for different grain geometries, the characterization of it by a proper parameter has not been very successful [11, 14].

It is well established that failure of polycrystalline materials at creep regime is often associated with the nucleation and growth of cavities at the grain boundaries. It has been conclusively shown that cavity nucleation at the grain boundaries occurs more readily than other mechanisms, such as slip band impingement, due to the development of high stresses resulting from grain boundary sliding [16, 17]. The studies on the effects of grain boundary sliding on cavity growth have shown that the cavity growth rate is substantially higher in the presence of grain boundary sliding [13, 18, 19].

The creep deformation behaviour of composites significantly differs from that of polycrystalline matrix material. Although the creep rupture times are usually much longer in the composites, they usually exhibit larger creep exponent or stress dependent creep exponent values (i.e. n values change above a certain applied stress level at the same testing temperature) [20–23]. A much larger scale creep cavitation at the triple grain boundary junctions during the creep deformation of the composites has also been reported [21–24].

In this study, in order to elucidate the grain boundary sliding behaviour in discontinuously reinforced composites, a series of numerical analyses were carried out. The results obtained are compared to the creep deformation of polycrystalline matrix material having identical grain morphology.

2. Details of the fem analyses

In the present analyses the matrix was modelled as a unit-cell of an array of two dimensional plane-strain hexagonal grains as shown in Fig. 1a. On the other hand, for the composite, with a 20% volume fraction of reinforcement, a unit-cell around the periodic array of aligned discontinuous reinforcements within the two dimensional grains as shown in Fig. 1(b–d) was employed. The grain sizes and the grain shapes were identical for both the matrix case (Fig. 1a) and the composite cases (Fig. 1(b–d)). While the volume fraction of the reinforcement and the grain shape were kept constant, the reinforcement aspect ratio (length to width ratio, l_f/r_f) was varied between 2.5–10 in

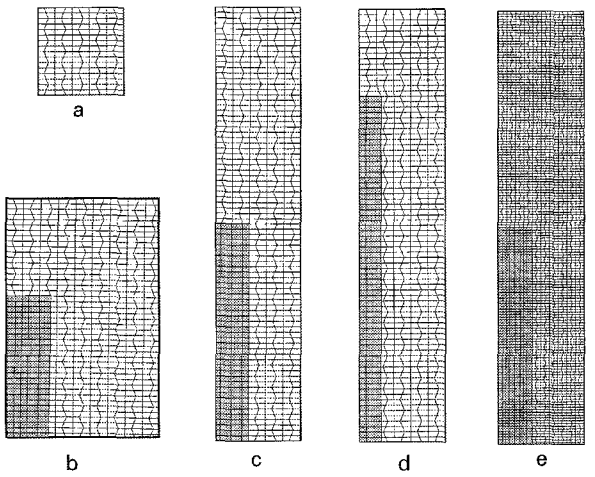

Figure 1 The FEM model used in the analyses. a)-FEM model for polycrystalline matrix, (b–d)-FEM model for the composite behaviour with reinforcement aspect ratios of 2.5, 5 and 10 respectively and (e)-FEM model for composite behaviour with a smaller matrix grain size and with reinforcement aspect ratio $l_f/r_f = 5$. The dark regions in the figures are the reinforcements.

Figs. 1(b–d). In order to elucidate the role of grain size on the grain boundary sliding behaviour of the composites, the grain size was reduced by a factor of four while maintaining identical grain shape, Fig. 1e. For this case the reinforcement aspect ratio was also kept as 5. In order to clearly reveal the grain structure, the triangular linear displacement elements have been omitted from Fig. 1. In the original FEM meshes, each rectangular region seen in Fig. 1 was divided into four rectangular regions and each resulting rectangle was further subdivided into four triangular linear displacement elements. Thus each grain seen in Fig. 1 was modelled by 128 triangular elements. The grain boundaries were considered to be free to slide. To simulate the free boundary sliding, the corresponding nodes on both sides of a grain boundary were constrained to have the same displacements in the direction normal to the grain boundary but were otherwise free to move in the local tangential direction. The nodes of three adjacent grains at triple points were constrained together in all normal directions but again free to slide in local tangential directions to meet the compatibility conditions. In this study, unless otherwise indicated, during the analyses of the composite behaviour the grains next to the reinforcement were rigidly connected to reinforcement providing a nonsliding interfacial behaviour between the reinforcement and the matrix. The deformation of the unit-cell must be constrained to maintain the compatibility and equilibrium with the adjacent material. This constraint requires that the cell boundaries remain straight and orthogonal, and free of shear traction. Several methods for imposing these requirements on the FEM models have been suggested; the procedure outlined in [25] was utilized in this study.

The FEM program has been developed which follows the formulation of Kanchi *et al.* [26]. For this study, an implicit time stepping procedure was used with variable time increments. The time steps were chosen according to the stability criterion proposed

by Cormeau [27] in order to avoid numerical instabilities. During the analyses the creep behaviour of the interior of the grains was assumed to obey Equation 1. The value of n was taken as $n = 2$, $1/\dot{\varepsilon}_0$ provides a natural time scale during the solution and applied stress values were normalized with σ_o. Furthermore, Young's modulus relating the elastic strain increments for the matrix material was taken as $E_m = 10^3\sigma_o$. In the case of the composites the Young's modulus of the reinforcement was assumed to be $E_f = 5E_m$ and the reinforcement remained elastic during the course of creep deformation. For both the matrix and the reinforcement, Poisson's ratio was chosen as $\nu = 0.3$. To simulate the constant-load creep test, normal traction was applied at the beginning of the solution to the end of the unit-cells such that the area integral of the traction was equal to the applied load:

$$\int_A T_i dA = \sigma A \tag{3}$$

3. Results

In the composites, for different reinforcement aspect ratios, the evolution of the stress fields in the continuum scale during the initial loading (i.e. at time $t = 0$) is shown in Fig. 2. As can be seen, the axial stress carried by the reinforcement is much larger than that carried by the matrix; also, the magnitude of the axial stress carried by the reinforcement is largest for the largest aspect ratio. Near the reinforcement ends within the matrix, the development of large stress components caused by the stress concentration effect of sharp corners of the reinforcement can also be seen in Fig. 2. Although the applied stress is uniaxial tension, a trixial-stress state develops. The transverse stress component takes a negative value between the reinforcements, while the regions at the tip of the reinforcements exhibit a positive value. The creep hardening behaviour of the discontinuous reinforced composites deforming with a power-law is associated with this formation of the triaxial stress state as discussed in detail in an earlier study [8].

The distribution of the stress components within the grains of the polycrystalline matrix material (Fig. 1a) during the initial loading is given in Fig. 3. Due to grain boundary sliding, the deformation is no longer homogeneous throughout the grains even though the applied stress is uniaxial tension. As can be seen from Fig. 3, the distribution is periodic with the extreme values occurring at the triple points for all the stress components. The contour values clearly show the positive and negative stress concentrations at the 60 and 120 degree sectors of the grain boundary. Although it is not resolved in Fig. 3, all the stress components are singular at the triple points as determined by asymptotic analysis [27]. In the case of the composites this periodic distribution of the stress components will be lost and it will be different for each grain depending on its location in the unit-cell of the composite (Fig. 1(b–d)) due to the large variation of the stresses at the continuum scale as shown earlier (Fig. 2).

In order to elucidate the creep behaviour in the absence of grain boundary sliding of the composites the initial analyses were carried out at the continuum scale. An example of such calculations at a normalized applied load level ($\sigma_{app}/\sigma_o = 1$) is shown in Fig. 4. In the figure, the strain rates observed during the creep deformation were normalized with the steady state strain rate value of the polycrystalline matrix material. As can be seen, under identical loading, both the time required to achieve the steady state and the steady state creep rates were affected by the reinforcement aspect ratio even though the volume fraction in the composites was the same. Larger reductions in steady state creep rates over that of polycrystalline matrix material occurred with increasing aspect ratio. This behaviour is the result of the evolution of nonuniform stress fields in the composites and their variation with reinforcement aspect ratio as shown earlier (Fig. 2). The variations in the creep strain rates with the inclusion of grain boundary sliding for each reinforcement aspect ratio are also indicated in Fig. 4. As can be seen, for all reinforcement aspect ratios the steady state creep rates were higher for the composites having sliding grain boundaries. These differences are quantified in the following section with the results obtained at other applied stress levels. During the analyses, at all applied stress levels the solutions were carried out well into the steady state at which the creep deformation rate becomes constant as seen in Fig. 4.

In Fig. 5, the variation of steady state creep rates for freely sliding grain boundaries at different applied stress levels are compared with nonsliding behaviour of both the polycrystalline matrix material and the composites having different reinforcement aspect ratios. In these simulations a nonsliding interfacial behaviour between the reinforcement and surrounding grains was assumed. In the case of polycrystalline matrix material with sliding grain boundaries, at low stress levels and low strain rate regime, the creep strain rates were higher and the observed strain rate values agree well with the estimated value by using stress enhancement factor, f, of 1.14 for $n = 2$ [10, 11] as indicated in the figures. With increasing applied stress levels, the contribution of grain boundary sliding to the creep deformation rate becomes smaller, and observed steady state creep rates approached the values predicted from creep constitutive equation (i.e. Equation 1) for the matrix material. In the composite cases, the contribution of grain boundary sliding increased with increasing aspect ratio (Fig. 5); this behaviour is summarized in terms of variations in the stress enhancement factor, f, in Fig. 6. In this figure, the dotted line at $f = 1.14$ was the value estimated in earlier studies [10, 11] as the stress enhancement factor of the polycrystalline matrix material having a creep exponent $n = 2$. The contribution of grain boundary sliding to the overall creep deformation is reduced as the f values approach unity, as can be seen in Fig. 6; this occurred at a very small stress range for the polycrystalline matrix material. The contribution of grain boundary sliding to creep deformation was significantly higher in the composites, and this contribution increased with increasing reinforcement aspect ratio

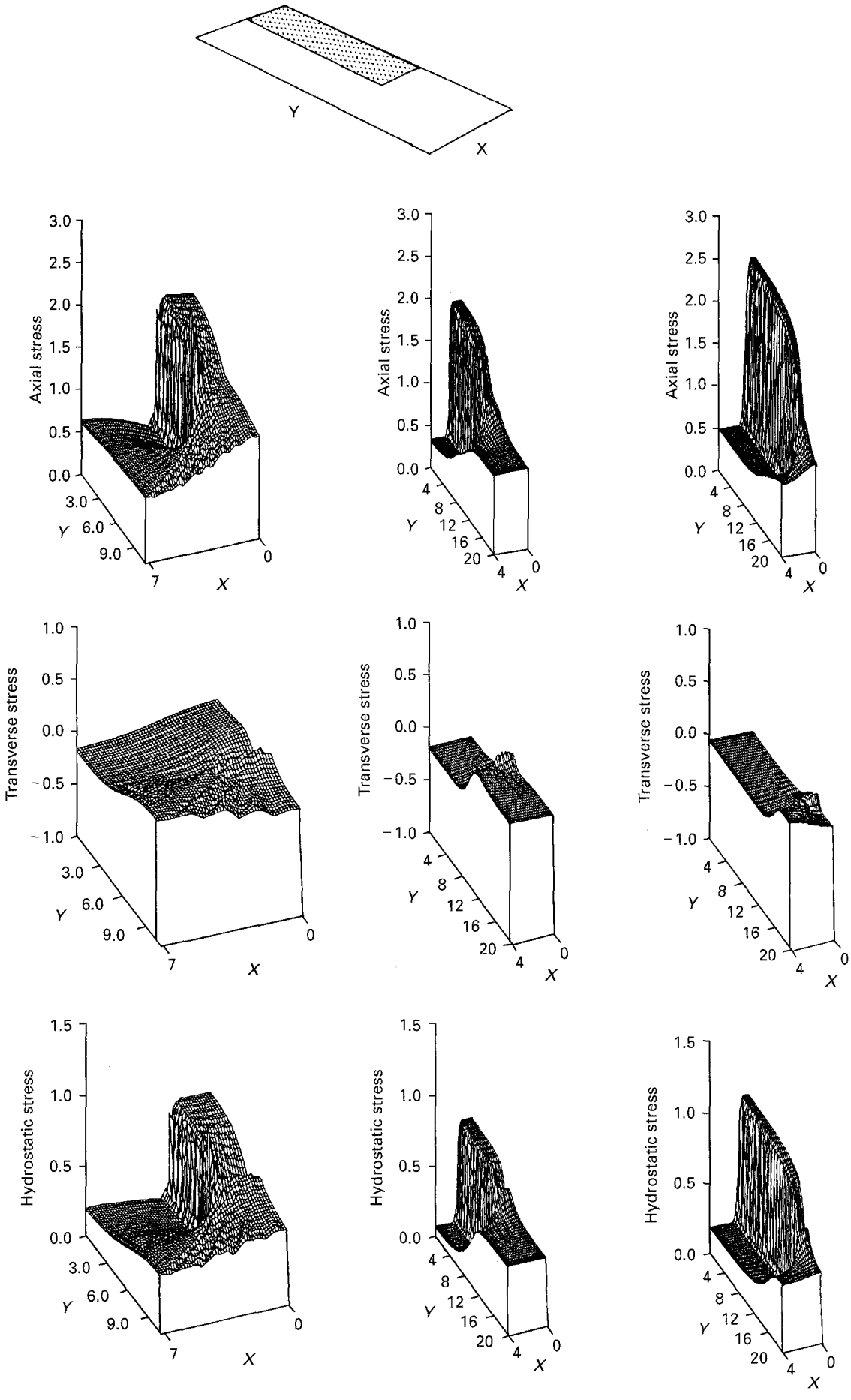

Figure 2 Distribution of stress components in the composite unit-cells at time $t = 0$. Top row is the axial stress distribution, middle row is the transverse stress distribution and bottom row is the hydrostatic stress distribution. Reinforcement aspect ratio (l_f/r_f) increases from left to right from 2.5 to 10 and the orientation of the reinforcement is indicated at the top of the figure.

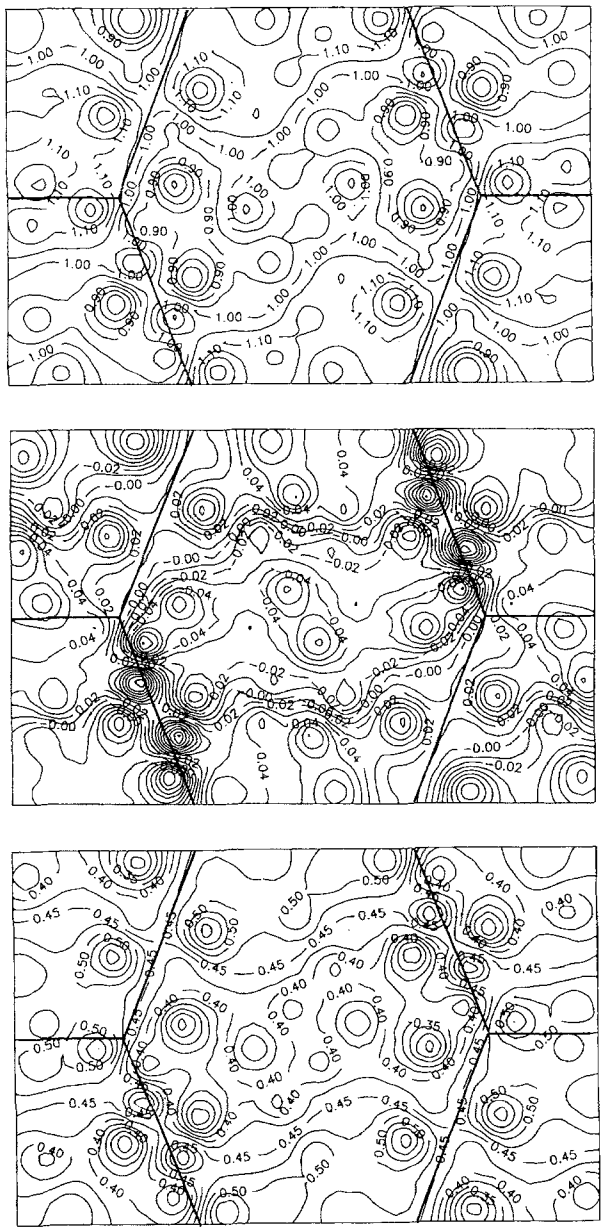

Figure 3 Distribution of stress components in the grains of polycrystalline matrix with sliding grain boundaries. Top is the axial stress distribution, middle is the transverse stress distribution and bottom is the hydrostatic stress distribution.

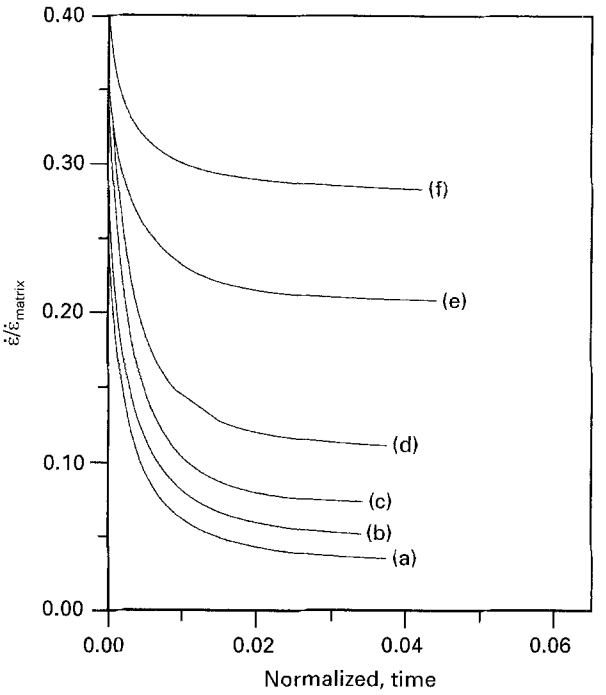

Figure 4 Variation of the creep strain rates with time at applied stress level (σ_{app}/σ_o) of one for composite with different aspect ratios. The strain rates in the figure were normalized with the steady state strain rate of the polycrystalline matrix material at an identical applied load level. The data were taken for l_f/r_f values of; (a) 10, (b) 10 (sliding), (c) 5, (d) 5 sliding, (e) 2.5 and (f) 2.5 sliding.

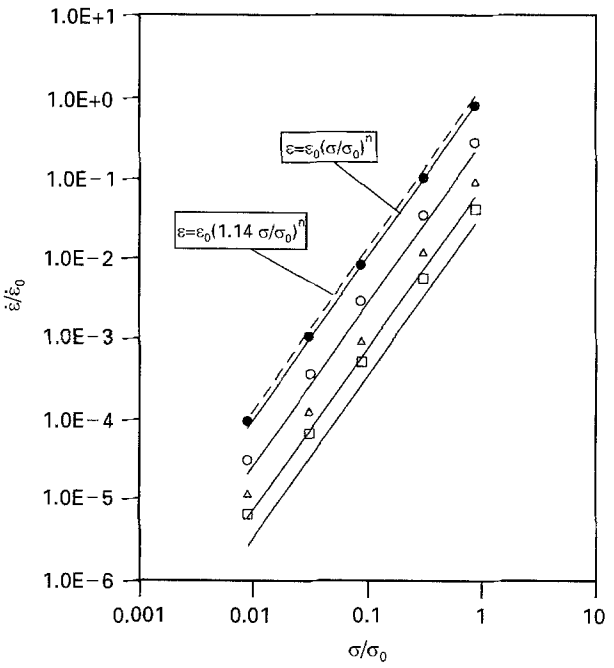

Figure 5 Comparison of the steady state creep strain rates with applied stress for grain boundary sliding and nonsliding cases for, (●) the matrix, (○) the composite with $l_f/r_f = 2.5$, (△) the composite with $l_f/r_f = 5$, (□) the composite with $l_f/r_f = 10$. The unbroken line represents data without grain boundary sliding.

as can be seen in Fig. 6. In the composites, this contribution also occurred over a much wider stress range in comparison to matrix material having identical grain morphology. The f values are still as high as 1.2 at the highest stress levels. Furthermore, grain boundary sliding did not significantly change the creep exponents of the composites (Fig. 5) and they were almost identical to that of the polycrystalline matrix material.

The typical creep displacement fields under a far field uniform tensile stress for a polycrystalline matrix material (Fig. 1a) are shown in Fig. 7. The grain boundary sliding on the vertical grain boundaries with broken horizontal lines can be easily identified. In contrast, the absence of grain boundary sliding on the horizontal grain boundaries can be seen from the continuity of the vertical lines. The overall creep displacement fields in the composites with different reinforcement aspect ratios at identical applied load levels are shown in Fig. 8. The formation of a nonuniform displacement field in the composites can be clearly seen: while the grains around the reinforcement exhibited large rotations as a result of vertical and horizontal grain boundary sliding, at regions away from the reinforcement the sliding behaviour was relatively more uniform. To further elucidate this nonuniform deformation behaviour resulting from grain boundary

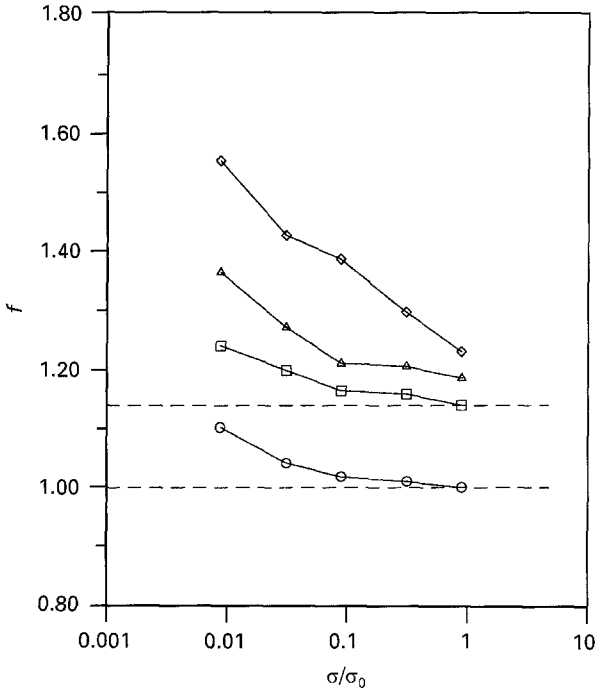

Figure 6 Variation of the stress enhancement factors for the polycrystalline matrix material and for the composites with different reinforcement aspect ratios. The matrix data is represented by the symbol (○) and the composites by, (□) with an l_f/r_f of 2.5 (△) with an l_f/r_f values of 5 and (◇) with an $l_f/r_f = 10$.

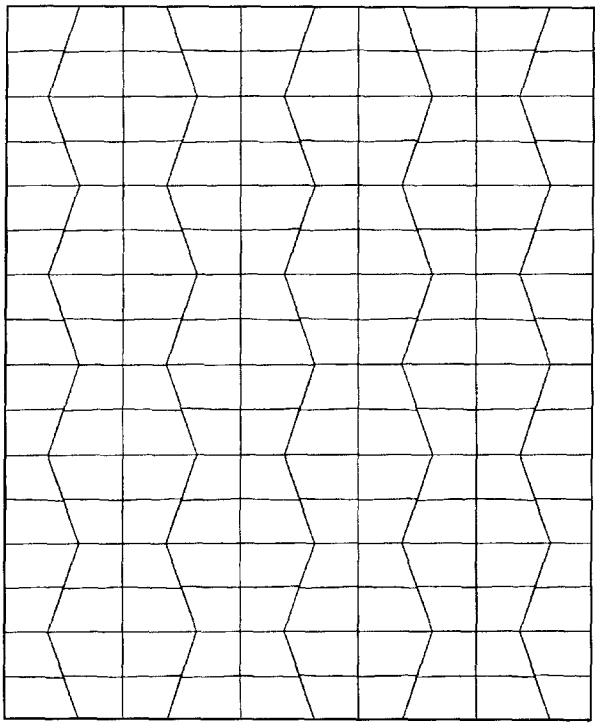

Figure 7 Creep displacement field under a far field uniform tensile stress for a polycrystalline matrix with sliding grain boundaries.

sliding, the normalized displacement vectors at steady state are shown in Fig. 9. It is apparent from the figure that both the magnitude of the rotations and the extent of the regions experiencing large rotations increased with increasing reinforcement aspect ratio. Of course, this behaviour is associated with the influence of the reinforcement aspect ratio on the evolution of the triaxial stress state as indicated earlier (Fig. 2).

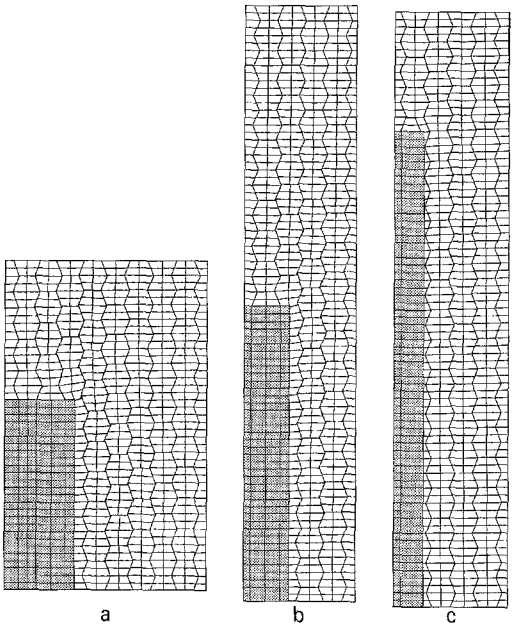

Figure 8 Creep displacement field under a far field uniform tensile stress for composites with sliding grain boundaries, a) reinforcement aspect ratio 2.5 b) reinforcement aspect ratio 5 and c) reinforcement aspect ratio 10. The dark regions are the reinforcements.

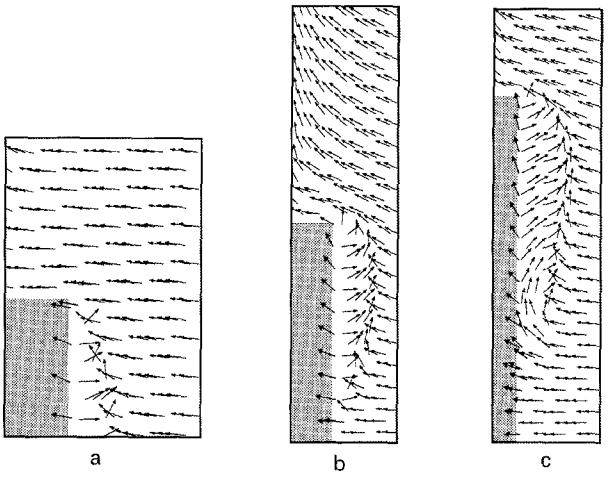

Figure 9 The distribution of displacement vectors in the composites with sliding grain boundaries, a) reinforcement aspect ratio 2.5 b) reinforcement aspect ratio 5 and c) reinforcement aspect ratio 10. The dark regions are the reinforcements.

In the following simulations the role of the grain size and the role of the interfacial behaviour between the reinforcement and the matrix were investigated. In these simulations the reinforcement aspect ratio was kept as 5. To determine the role of the grain size, the grain size was reduced by a factor of 4 while keeping the same grain morphology as shown in Fig. 1e. Furthermore, for this case the interface between the reinforcement and matrix was again assumed to be nonsliding. To simulate the sliding interfacial behaviour, the FEM mesh in Fig. 1c was utilized by introducing sliding boundary conditions around the reinforcement. For these last cases, the resulting steady state creep strain rates with applied stress are compared in Fig. 10. As can be seen from the figure, for the composites having identical reinforcement morphology (i.e., same aspect ratio and nonsliding interfacial

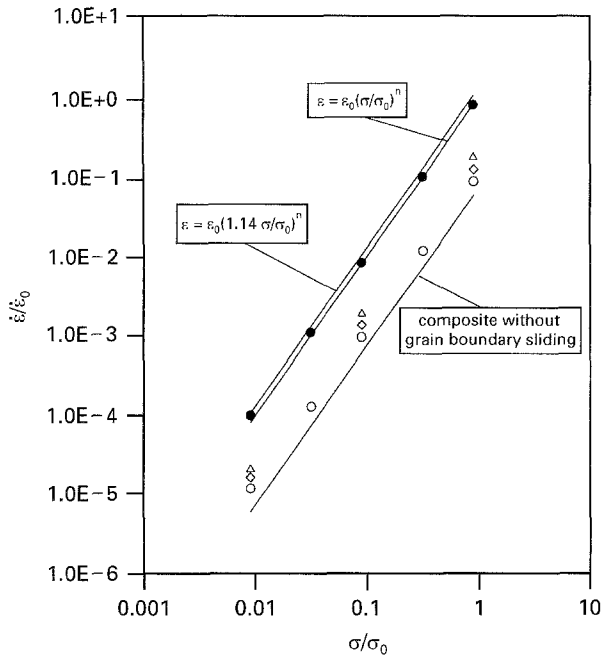

Figure 10 Comparison of the steady state creep strain rate with applied stress for small grain size and sliding interfacial behaviour between the reinforcement and the matrix cases. All the data was obtained at a reinforcement aspect ratio of 5 for; (●) the matrix, (○) the composite, (△) the composite with a sliding interface and (◇) a composite with small grain size.

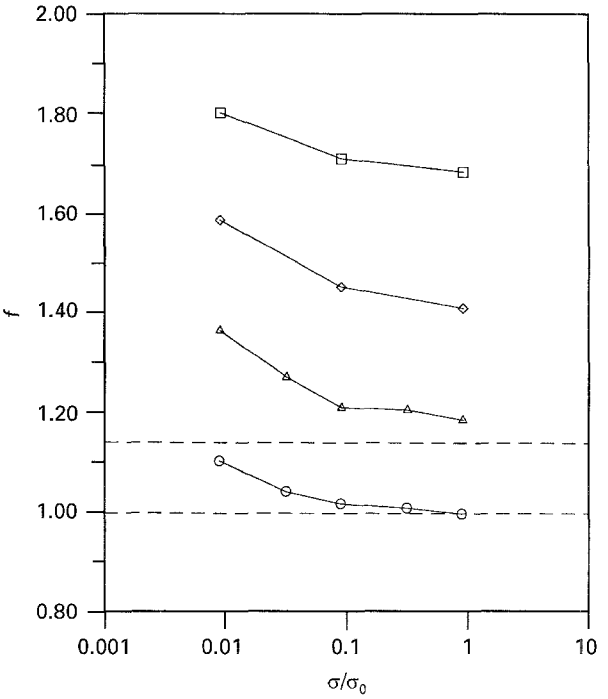

Figure 11 Variation of the stress enhancement factors in the composites with variation in the matrix grain size and sliding interfacial behaviour between the reinforcement and the matrix. The data is for; (○) matrix, (△) composite, (□) composite with sliding interface and (◇) composite with small grain size.

behaviour) the steady state creep rates were higher for the composite having smaller grain size. On the other hand, for the case of identical grain size and reinforcement aspect ratio, the sliding interfacial behaviour between the reinforcement and the matrix resulted in the highest creep rates for the composite. Again for these cases, the creep exponents for the composite did not change and they were almost identical to the creep exponent of the polycrystalline matrix material. The resulting stress enhancement factors from these simulations are given in Fig. 11. Although earlier studies have suggested that the stress enhancement factor for a polycrystalline material is independent of grain size, it appears that in the case of the composites the grain size has an influence and for a given reinforcement morphology, the f value increased with decreasing grain size. However, this increase does not appear to be proportional to the grain size. Although the over all creep rates were still significantly lower than the creep rates seen for the matrix material (Fig. 10), the interfacial behaviour between the matrix and the reinforcement appears to be the strongest influence on the stress enhancement factor for a given matrix grain size and reinforcement morphology. The resulting creep displacement fields for these cases are shown in Fig. 12. A comparison may be made between the nonsliding and sliding interfacial behaviour between the reinforcement and the matrix (Fig. 12(a, b)); in the case of a sliding interface, the limited amount of grain rotations in a very localized region, and large sliding of the grains along the interface without a large degree of rotation can be differentiated in Fig. 12b. On the other hand, a much larger degree of grain rotation and its spread to much wider regions along the reinforcement for the composite having a nonsliding interface but a smaller grain size is apparent in Fig. 12c.

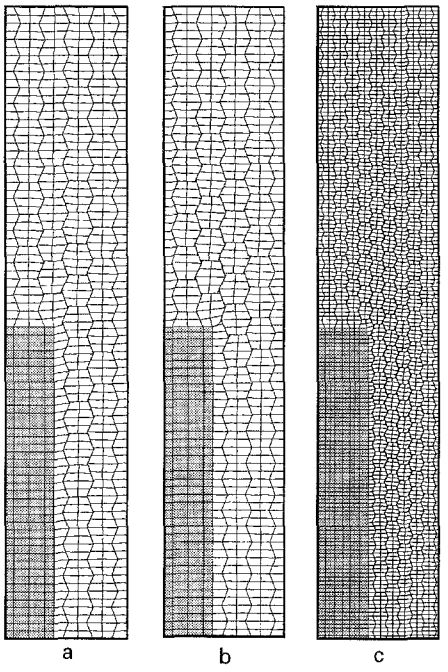

Figure 12 Creep displacement field under a far field uniform tensile stress for the composite with reinforcement aspect ratio 5, a) nonsliding interface between the reinforcement and the matrix, b) sliding interfacial behaviour between the reinforcement and the matrix, c) composite with smaller grain size and nonsliding interface between the reinforcement and the matrix.

Finally, an enlarged view of the section around the reinforcement in Fig. 12b is given in Fig. 13, in order to demonstrate the resulting cavitation at the triple

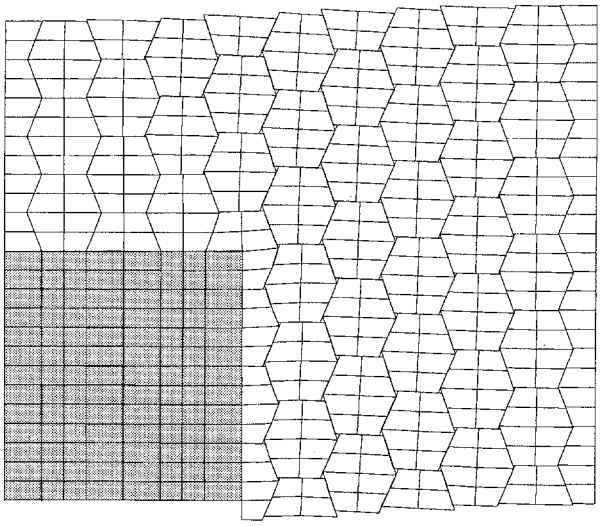

Figure 13 Enlarged view of Fig. 12b to reveal the details of grain rotation and triple point cavitation in the composites.

points due to unaccommodated grain rotation resulting from grain boundary sliding. This result clearly indicates one of the possible reasons for the experimentally observed high degree of triple point grain boundary cavitation in the composites (21–23).

4. Discussion

The present study of grain boundary sliding effects employing two dimensional plane-strain hexagonal grains is clearly only an approximation of a real polycrystalline material. Also, in the unit-cell analysis of the composite behaviour the assumptions of fully aligned reinforcement and completely periodic pattern of distribution are an idealization. Similarly, only grain arrangements as shown in Fig. 1(b–e) at the interface region between the reinforcement and the surrounding matrix grains were assumed for the composites. The thermal stresses due to the differences in thermal expansion coefficients of the phases were also neglected during the analysis.

In this study, the stress enhancement factor observed for the polycrystalline matrix material agrees closely with the results given earlier [10, 11] (Fig. 6). In the composite cases, the stress enhancement factors observed were higher than the one seen for the polycrystalline matrix material having an identical grain morphology. For a given reinforcement volume fraction, the geometric parameters of the reinforcement (i.e. aspect ratio) appear to have a strong influence on the creep deformation behaviour of composites with sliding grain boundaries. The observed stress enhancement values for the composites increased with increasing reinforcement aspect ratio. Also, the contribution of the grain boundary sliding to creep deformation rate of the composites took place in a much larger stress range in comparison to that seen for the matrix material (Fig. 6). Although the earlier studies have suggested that the stress enhancement factor for a polycrystalline material is independent of the grain size but may depend on the geometrical parameters related to the grain shape, in this study, an influence of the grain size on the creep deformation rate was also observed. The stress enhancement factor of the composite was further increased with decreasing grain size for a given reinforcement morphology (Fig. 11). However, this increase seems not to be proportional to the grain size. For a given grain morphology and reinforcement aspect ratio, the interfacial behaviour between the matrix and the reinforcement appears to have strongest influence on the creep deformation rate. For sliding interfaces between the reinforcement and the matrix, although steady state creep rates was still significantly lower than the ones seen for the matrix material (Fig. 10), this interfacial sliding contributed significantly to overall composite creep rate (Fig. 11). All these observed larger contribution of the grain boundary sliding behaviour to the over all composite creep rates (Figs 6 and 11), of course is associated with the development of large triaxal stress state in the composites, the stress concentration of effect at the reinforcement ends (Fig. 2) and due to large grain rotations resulting from the grain sliding (Figs 7–9 and 11).

Many composite systems usually exhibit larger creep exponent or stress dependent stress exponent values (i.e. n values change above a certain applied stress level at the same testing temperature) than their constituent matrix material [20–23]. This behaviour is usually attributed to grain sliding and/or interfacial sliding between the reinforcement and the matrix in the composites. However, in all the cases investigated in this study, the observed creep exponent values for the composites remained almost identical to that seen for the polycrystalline matrix material (Figs 4 and 10). It appears that the experimentally observed larger creep exponent values or stress dependent creep exponent values for the composites could not be explained solely by the mechanism of grain boundary sliding. On the other hand, the experimentally observed large scale triple point grain cavitation in the composite could occur as a result of unaccomodated large grain rotation originating from grain sliding as seen in Fig. 13.

Rodin and Dib [15] have performed FEM analysis for determination of stress enhancement factor using three dimensional Wigner–Seitz unit-cells for a polycrystalline material. Their analyses have shown larger values of stress enhancement factor but decreasing behaviour with creep exponent (1.31 to 1.23 for $1 \leqslant n \leqslant 7$). Although, the stress enhancement factor has been evaluated by several authors for different grain geometries, the characterization of it by a proper parameter has not been successful [11–14]. Therefore, it is expected that the contribution of grain boundary sliding to the creep deformation characteristics of the discontinuously reinforced composites will be somewhat higher than the ones elucidated in this study. In spite of the above mentioned simplifications, present results clearly show the differences in the grain boundary sliding behaviour between a polycrystalline matrix material and a discontinuous reinforced composite both having identical grain size and morphology. The results also indicate the significant role of the other

microstructural parameters, such as interfacial behaviour between the reinforcement and the matrix and the matrix grain size, on the creep behaviour of such composites.

5. Conclusions

In this study, grain boundary sliding behaviour in a discontinuously reinforced composite and a polycrystalline matrix having identical grain morphologies was investigated together with the other influencing parameters: reinforcement aspect ratio, grain size and interfacial behaviour between the reinforcement and the matrix. The results indicate that:

(1) The stress enhancement factor for the composites is much higher than the one observed for the matrix material and its value increases with increasing reinforcement aspect ratio, reduction in the matrix grain size and sliding interfacial behaviour between the reinforcement and the matrix.

(2) In the composites, the contribution of the grain boundary sliding to overall steady state creep rates occurs in a larger stress range in comparison to the matrix material.

(3) Experimentally observed larger creep exponent values or stress dependent creep exponent values for the composites could not be explained solely by the mechanism of grain boundary sliding.

(4) Experimentally observed large scale triple point grain boundary cavitation in the composites could occur due to large grain rotations resulting from grain boundary sliding and evolution of triaxial stress state.

Acknowledgements

This work was performed for the United States Department of Energy by Iowa State University under contract W-7405-Eng-82. This research was supported by the Director of Energy Research, Office of Basic Energy Sciences.

References

1. P. F. BECHER, *J. Amer. Ceram. Soc.* **6** (1991) 255.
2. J. W. HOLMES, *J. Mater. Sci.* **26** (1991) 1808.
3. T. C. LU, A. G. EVANS, R. J. HECT and R. MEHRABIAN, *Acta Metall.* **39** (1991) 1853.
4. "Advanced Metal Matrix Composites For Elevated Temperatures", edited by M. N. Gungor, E. J. Lavernia and S.G. Fishman, (ASM, International Materials Park OH. 1991)
5. "Fundamental Relationships Between Microstructure and Mechanical Properties of Metal Matrix Composites", edited by M. N. Gungor and P. K. Liaw (Metallurgical Society of AIME, Warrandale PA. 1990)
6. J. LLORCA, A. NEEDLEMAN and S. SURESH, *Acta Metall.* **39** (1991) 2317.
7. T. L. DRAGONE and W. D. NIX, *ibid.* **38** (1990) 1941.
8. S. B. BINER, *Mat. Sci Engng.*, **A156** (1992) 21.
9. F. W. CROSSMAN and M. F. ASHBY, *Acta Metall. Mater.* **23** (1975) 425.
10. F. GRAHMANI, *Int. J. Solids Struct.* **16** (1980) 825.
11. K. J. HSIA, D. M. PARKS and A. S. ARGON, *Mech. Mat.* **11** (1991) 43.
12. E. W. HART, *Acta Metall. Mater.* **15** (1967) 1545.
13. I. W. CHEN and A. S. ARGON, *ibid.* **27** (1979) 749.
14. P. M. ANDERSON and J. R. RICE, *ibid.* **33** (1985) 409.
15. G. J. RODIN and M. W. DIB, in "Advances in Fracture Research" edited by K. Salama and K. Upadhya, Vol. 2, (Pergaman Press, Oxford, 1989) p. 835.
16. A. S. ARGON; in "Recent Advances in Creep and Fracture of Engineering Materials and Structures" edited by B. Wilshire and D. R. J. Owen (Pineridge Press, Swansea 1982), p. 1.
17. H. RIEDEL, *Acta Metall. Mater.* **32** (1984) 313.
18. V. TVERGAARD, *J. Mech. Phys. Solids* **32** (1984) 373.
19. *idem, ibid,* **33** (1985) 447.
20. E. VEN DER GIESSEN and V. TVERGAARD, *Int. J. Fracture* **48** (1991) 153.
21. S. B. BINER and W. A. SPITZIG, *Mat. Sci. Engng.* **A150** (1992) 213.
22. T. G. NIEH, *Metall. Trans.* **15A** (1984) 139.
23. H. T. LIN and P. F. BARKER, *J. Amer. Ceram. Soc.* **74** (1991) 1886.
24. A. H. GHOSKI and J. R. PORTER, *ibid* **68** (1985) C-144.
25. R. E. SMELSER and R. BECKER, In Abaques Users Conference Proceedings; edited by H. Hibbitt, C. Karlson and D. J. Sorensen (HKS Inc. Rhode Island 1990) p. 207.
26. M. B. KANCHI, O. C. ZIENKIEWICZ and D. R. J. OWEN, *Int. J. Num. Meth. Eng.* **12** (1975) 109.
27. I. CORMEAU, *ibid* **8** (1974) 461.
28. C. W. LAU, A. S. ARGON and F. A. McCLINTOCK, in "Elastic–Plastic Fracture Mechanics" edited by C. F. Shih and J. P. Gudas ASTM–STP803, (ASTM Philadelphia PA. 1983). p. 551.

Received 28 June 1995
and accepted 21 December 1995